# Subwavelength ultrasonic circulator based on spatiotemporal modulation

Romain Fleury, Dimitrios L. Sounas, and Andrea Alù*

*Department of Electrical and Computer Engineering, The University of Texas at Austin, Austin, Texas 78712, USA*

(Received 6 February 2015; revised manuscript received 17 March 2015; published 28 May 2015)

Enabling efficient nonreciprocal acoustic devices is challenging, yet very desirable for a variety of applications, including acoustic imaging, underwater communications, energy concentration and harvesting, signal processing, and noise control. We discuss the theory and design of a fully linear compact acoustic circulator based on spatiotemporal modulation of the effective acoustic index, providing a compact and practical way to realize large sound circulation at any desired frequency. Our proposal enables tunable isolation levels of over 40 dB, with insertion losses as low as 0.3 dB, in a noise-free, integrable, frequency scalable device whose total size does not exceed $\lambda/6$.

DOI: 10.1103/PhysRevB.91.174306 PACS number(s): 43.20.−f, 03.65.Ge, 43.35.−c

## I. INTRODUCTION

In wave physics, reciprocity is a property directly related to the fundamental symmetry of wave propagation, according to which transmission between two points in space is independent on the direction of propagation, and it directly stems from the invariance of wave propagation upon time reversal. There are applications in which one would like to break reciprocity and obtain one-way wave transmission, for instance in order to protect a source from unwanted load reflections. The first reciprocity relations were introduced in 1856 by Von Helmholtz [1], and further developed by Lord Rayleigh in the particular case of acoustic waves [2]. However, practical devices that can significantly break reciprocity have been for a long time exclusively realized for electromagnetic waves using magnetically biased ferrites based on the Faraday effect [3], leading to the development of Faraday isolators, a technology that is widely used in nowadays communication systems. Because of the relatively weak interaction between elastic waves and a dc magnetic field in magnetoacoustic crystals [4], obtaining strong magnetically induced acoustic nonreciprocity is quite challenging [5], and until recently no solution for large acoustic signal isolation in a compact device existed.

The conditions under which Rayleigh reciprocity theorem holds can be broken in three different ways: (i) breaking linearity, (ii) biasing with a quantity that is odd under time reversal, or (iii) breaking time invariance [6,7]. Large acoustic isolation has been obtained using option (i) in a nonlinear medium paired with a frequency selective mirror [8,9], or with the help of nonlinear acoustic inclusions [10]; however, all these nonlinear solutions typically introduce severe signal distortions and only work for large acoustic intensities. According to the Onsager-Casimir principle of microscopic reversibility [11], linear isolation is possible if the system is biased with an odd vector upon time reversal, just like the static magnetic field in the case of the Faraday isolator [option (ii)]. Following this principle and using angular momentum as the biasing vector, we have recently proposed large nonreciprocity at audible frequencies in an acoustic circulator constructed with a resonant ring cavity filled with an internal fluid in a constant rotating motion [12]. A drawback of this method is the practical challenge to implement at higher frequencies such mechanical motion, as the size of the resonator shrinks. In addition, this method may not be directly applicable to other types of mechanical waves, such as structural surface waves, for which the possibility to break the reciprocal nature of their propagation may lead to novel venues in energy manipulation, concentration, and harvesting.

In this article we propose a practical route towards linear, noise-free, ultrasonic acoustic isolation through an effective rotation of a subwavelength ultrasound circulator obtained via parametric modulation. Consider the geometry in Fig. 1 (top): three cylindrical acoustic cavities are connected to each other via small channels, forming an acoustic resonator with 120° rotational symmetry. Three additional channels couple this resonator to external waveguides, defining a three-port network. We break reciprocity by applying suitable spatiotemporal modulation to the cavity volumes with modulation frequency $f_m = \omega_m/(2\pi)$. This modulation is applied in a rotating fashion: the volume $V_0$ of cavity 1 is modulated by an amount $\Delta V_1 = \delta V \cos(\omega_m t)$, whereas the volumes of cavities 2 and 3 are modulated at the same frequency $f_m$ and strength $\delta V$, but with $2\pi/3$ and $4\pi/3$ phase delays, i.e., $\Delta V_2 = \delta V \cos(\omega_m t - 2\pi/3)$ and $\Delta V_3 = \delta V \cos(\omega_m t - 4\pi/3)$, respectively. Because of this dynamic modulation, the system is no longer time invariant, and time-reversal symmetry is broken by the effective angular momentum imparted by the modulation, violating the assumptions of Rayleigh reciprocity theorem, and possibly leading to strong nonreciprocal effects. An analogous functionality was achieved for radio waves in a parametric lumped circuit in [13], and we now translate these concepts to acoustic propagation.

## II. THEORY

### A. Lumped circuit model equivalent

The behavior of the proposed device can be predicted in the low frequency limit by considering its lumped circuit model equivalent. In this limit we can assume that the acoustic pressure is constant within each of the three cavities, with pressure amplitudes $p_1$, $p_2$, and $p_3$. The three cavities can be modeled as parallel acoustic capacitors [Fig. 1 (bottom)], since they store potential acoustic energy and accumulate a net amount of pressure $p_i$, or acoustic voltage in the equivalent

*Corresponding author: alu@mail.utexas.edu

 

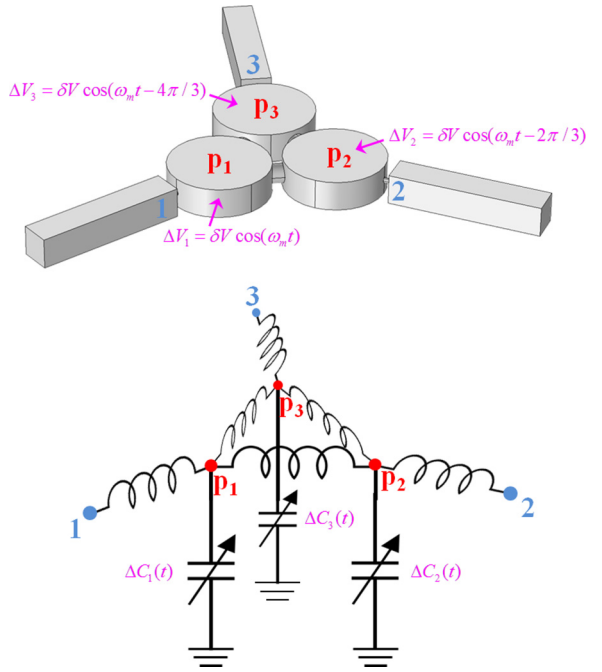


FIG. 1. (Color online) Geometry of the proposed three-port network. Top: Three acoustic cavities connected via small channels and coupled to three waveguides. The volumes $V$ of the cavities are weakly modulated *in a rotating fashion*, with amplitude $\delta V$ and frequency $\omega_m$. Bottom: Equivalent lumped circuit model in the long wavelength limit. The modulation of the physical volume of the cavity translates into a modulation of their acoustic compliance, represented here by variable shunt capacitors.

circuit, with respect to the static pressure $p_0$ represented by the ground in the circuit model. The difference in pressure stored by two adjacent cavities creates a force that acts on the mass of the fluid filling the small channel coupling them. Therefore, the elements connecting the three capacitors at nodes $p_1$, $p_2$, and $p_3$ behave as acoustic inductors of value $L$. The coupling to the external ports is also assumed to be of inertial, or inductive, nature, which is again represented by inductors connecting the nodes $p_1$, $p_2$, and $p_3$ to ports 1, 2, and 3. To take into account the modulation in the equivalent circuit of Fig. 1, we recall that the expression for the acoustic capacitance $C_0$ of a cavity in the long wavelength limit is given by $C_0 = V_0\beta_0$ [14], where $V_0$ is the unbiased cavity volume and $\beta_0$ is the compressibility of the acoustic medium filling it, taken here to be silicon rubber RTV-602, with density $\rho_0 = 990$ kg/m$^3$ and compressibility $\beta_0 = 9.824 \times 10^{-10}$ Pa$^{-1}$ [15]. Assuming that the volume modulation is obtained using actuators that compress the acoustic medium filling the cavities, and that the material is deformed elastically, the compressibility $\beta_0$ is untouched by the modulation, and therefore the actuators directly modulate the acoustic capacitance with modulation depth $\delta C/C_0 = \delta V/V_0$. This is represented in the equivalent circuit by variable capacitors.

### B. Temporal coupled-mode theory

In order to model the device and solve the scattering problem for a signal incident at one of the ports, we use temporal coupled-mode theory, which is essentially perturbation theory applied in the time domain. This theory is justified here as we assume weak modulation depth and low modulation frequency throughout the paper. The first step is to consider the resonant properties of the unbiased structure, before applying perturbation theory to include the effect of the modulation.

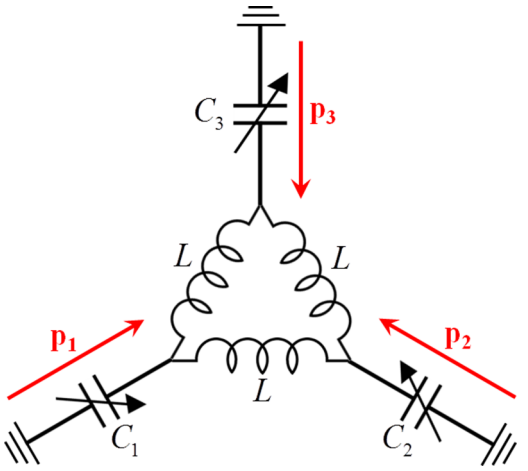


FIG. 2. (Color online) Lumped element model of the resonator alone.

Let us consider the unbiased resonator by itself, represented in Fig. 2. The capacitors have constant values $C_1 = C_2 = C_3 = V_0\beta_0$ and we do not consider at this point the coupling to ports 1, 2, and 3, i.e., there are no radiative losses. We start by applying Kirchhoff's laws to the circuit, obtaining

$$\begin{aligned} \frac{d^2p_1}{dt^2} &= \frac{1}{LC_0}(p_2 + p_3 - 2p_1), \\ \frac{d^2p_2}{dt^2} &= \frac{1}{LC_0}(p_3 + p_1 - 2p_2), \\ \frac{d^2p_3}{dt^2} &= \frac{1}{LC_0}(p_1 + p_2 - 2p_3). \end{aligned} \tag{1}$$

Next, we represent the acoustic state of the resonator by the three component vector

$$|\psi\rangle = \begin{pmatrix} p_1 \\ p_2 \\ p_3 \end{pmatrix}, \tag{2}$$

whose time evolution is obtained directly from (1) as

$$\frac{d^2}{dt^2}|\psi\rangle = M_0|\psi\rangle. \tag{3}$$

In (3) we have introduced the Hermitian time evolution operator

$$M_0 = \frac{1}{LC_0}\begin{pmatrix} -2 & 1 & 1 \\ 1 & -2 & 1 \\ 1 & 1 & -2 \end{pmatrix}. \tag{4}$$

We can transform (3) into the frequency domain eigenvalue problem

$$M_0|\psi\rangle = -\omega^2|\psi\rangle, \tag{5}$$

whose solutions are the three eigenmodes of the unbiased structure. The first one, with eigenvalue $\omega = 0$ and eigenvector

$$|0\rangle = \frac{1}{\sqrt{3}}\begin{pmatrix}1\\1\\1\end{pmatrix}, \tag{6}$$

is the dc mode, which expresses the capability of the cavity to store a uniform static pressure (at dc the capacitors are replaced by open circuits and the inductors by shorts, obtaining a node that is unconnected to the ground, whose voltage is arbitrary). The second and third modes, $|+\rangle$ and $|-\rangle$, are counter-rotating degenerate modes associated with the lumped resonance of the structure at $\omega_\pm = \sqrt{3/LC_0}$,

$$|+\rangle = \frac{1}{\sqrt{3}}\begin{pmatrix}1\\e^{i\frac{2\pi}{3}}\\e^{i\frac{4\pi}{3}}\end{pmatrix}, \tag{7}$$

$$|-\rangle = \frac{1}{\sqrt{3}}\begin{pmatrix}1\\e^{-i\frac{2\pi}{3}}\\e^{-i\frac{4\pi}{3}}\end{pmatrix}. \tag{8}$$

Next, we apply perturbation theory to the unbiased resonator. We assume that the values of the capacitors $C_1$, $C_2$, and $C_3$ are modulated by the amounts $\Delta C_1$, $\Delta C_2$, and $\Delta C_3$ in a rotating fashion, following

$$\begin{aligned} C_1 &= C_0 + \Delta C_1 = C_0 + \delta C\cos(\omega_m t),\\ C_2 &= C_0 + \Delta C_2 = C_0 + \delta C\cos(\omega_m t - 2\pi/3),\\ C_3 &= C_0 + \Delta C_3 = C_0 + \delta C\cos(\omega_m t - 4\pi/3), \end{aligned} \tag{9}$$

where $\omega_m$ and $\delta C = \beta_0 \delta V$ are, respectively, the modulation frequency and modulation depth. We further assume that the modulation is practically realizable, i.e., it is sufficiently weak and slow, $\delta C \ll C_0$ and $\omega_m \ll \omega_\pm$. Under these assumptions, Eq. (3) is replaced by

$$\frac{d^2}{dt^2}|\psi\rangle = (M_0 + \delta M)|\psi\rangle, \tag{10}$$

with

$$\delta M = -\frac{\delta C}{2C_0}\frac{\omega_\pm^2}{3}\begin{pmatrix} -2(e^{i\omega_m t}+e^{-i\omega_m t}) & e^{i\omega_m t}+e^{-i\omega_m t} & e^{i\omega_m t}+e^{-i\omega_m t}\\ e^{i(\omega_m t-2\pi/3)}+e^{i(\omega_m t-2\pi/3)} & -2(e^{i(\omega_m t-2\pi/3)}+e^{i(\omega_m t-2\pi/3)}) & e^{i(\omega_m t-2\pi/3)}+e^{i(\omega_m t-2\pi/3)}\\ e^{i(\omega_m t-4\pi/3)}+e^{-i(\omega_m t-4\pi/3)} & e^{i(\omega_m t-4\pi/3)}+e^{-i(\omega_m t-4\pi/3)} & -2(e^{i(\omega_m t-4\pi/3)}+e^{-i(\omega_m t-4\pi/3)}) \end{pmatrix}. \tag{11}$$

Applying perturbation theory, we expand at any instant $t$ the acoustic state $|\psi(t)\rangle$ in the biased cavity into the basis of eigenvectors of the unbiased time-evolution matrix $M_0$, obtaining

$$|\psi(t)\rangle = a_0(t)|0\rangle + a_+(t)|+\rangle + a_-(t)|-\rangle = \sum_i a_i(t)|i\rangle, \tag{12}$$

where $a_i(t)$ denotes the time-dependent amplitude of the mode $|i\rangle$. Plugging this expansion into (10), and considering the fact that the eigenmodes of $M_0$ have been normalized with respect to the scalar product

$$\langle\psi_a|\psi_b\rangle = p^*_{a,1}p_{b,1} + p^*_{a,2}p_{b,2} + p^*_{a,3}p_{b,3}, \tag{13}$$

we obtain the following differential equations for the mode amplitudes:

$$\begin{aligned} \frac{d^2}{dt^2}a_0 &= \langle 0|\delta M|0\rangle a_0 + \langle 0|\delta M|+\rangle a_+ + \langle 0|\delta M|-\rangle a_-,\\ \frac{d^2}{dt^2}a_+ &= -\omega_+^2 a_+ + \langle +|\delta M|0\rangle a_0 + \langle +|\delta M|+\rangle a_+ \\ &\quad + \langle +|\delta M|-\rangle a_-,\\ \frac{d^2}{dt^2}a_- &= -\omega_-^2 a_- + \langle -|\delta M|0\rangle a_0 + \langle -|\delta M|+\rangle a_+ \\ &\quad + \langle -|\delta M|-\rangle a_-. \end{aligned} \tag{14}$$

The matrix elements $\langle i|\delta M|j\rangle$ can be evaluated using (11) together with Eqs. (6)–(8) for the normalized eigenstates of $M_0$. We find that the modulation induces no coupling from the dc mode into the counter-rotating modes,

$$\langle +|\delta M|0\rangle = \langle -|\delta M|0\rangle = 0, \tag{15}$$

and that the diagonal matrix elements are null,

$$\langle 0|\delta M|0\rangle = \langle +|\delta M|+\rangle = \langle -|\delta M|-\rangle = 0. \tag{16}$$

However, the other matrix elements are nonzero and are calculated as

$$\langle 0|\delta M|+\rangle = \langle +|\delta M|-\rangle = \frac{\delta C}{2C_0}\omega_\pm^2 e^{i\omega_m t}, \tag{17}$$

$$\langle 0|\delta M|-\rangle = \langle -|\delta M|+\rangle = \frac{\delta C}{2C_0}\omega_\pm^2 e^{-i\omega_m t}. \tag{18}$$

Next, we make the assumption that the acoustic device is designed such that the values of $L$ and $C_0$ satisfy the following condition:

$$\omega_\pm = \sqrt{\frac{3}{LC_0}} \gg 0, \tag{19}$$

that is, the lumped resonance frequency of the structure is far from dc. If we assume that we excite the structure at a frequency $\omega$ close to $\omega_\pm$, and considering that $\omega_m \ll \omega_\pm$,

we conclude that coupling of energy between the counter-rotating modes and the dc mode is very inefficient (secular approximation). Under these conditions, the coupled-mode equations (14) simplify to

$$\begin{aligned}\frac{d^2}{dt^2}a_+ &= -\omega_\pm^2 a_+ + \chi e^{i\omega_m t}a_-,\\ \frac{d^2}{dt^2}a_- &= -\omega_\pm^2 a_- + \chi e^{-i\omega_m t}a_+,\end{aligned} \tag{20}$$

where $\chi = \omega_\pm^2 \delta C/(2C_0)$.

### C. Scattering parameters

To evaluate the scattering properties of the device, we now add coupling to the external ports, with decay rate $\gamma$, which is assumed to be constant over the frequency range of interest, and identical for both counter-rotating modes. This assumption is valid as long as the quality factor of the structure is large enough, which is the case here since the coupling channels to the ports are very narrow. We further note $S_i^+$ the incident signal at port $i$, and $S_i^-$ the outgoing one, and introduce the notation

$$\Omega_\pm = \omega_\pm + i\gamma. \tag{21}$$

Owing to energy conservation, 120° symmetry, and the time-reversal properties of the structure, Eq. (20) is modified to yield the full coupled-mode equations including decay and coupling to the ports:

$$\begin{aligned}\frac{d^2}{dt^2}a_+ &= -\Omega_\pm^2 a_+ + \chi e^{i\omega_m t}a_- \\ &\quad - 2i\omega_\pm\sqrt{\frac{2\gamma}{3}}(S_1^+ + e^{-i\frac{2\pi}{3}}S_2^+ + e^{-i\frac{4\pi}{3}}S_3^+),\\ \frac{d^2}{dt^2}a_- &= -\Omega_\pm^2 a_- + \chi e^{-i\omega_m t}a_+ \\ &\quad - 2i\omega_\pm\sqrt{\frac{2\gamma}{3}}(S_1^+ + e^{i\frac{2\pi}{3}}S_2^+ + e^{i\frac{4\pi}{3}}S_3^+).\end{aligned} \tag{22}$$

The outgoing signals are given by

$$\begin{aligned}S_1^- &= -S_1^+ + \sqrt{\frac{2\gamma}{3}}(a_+ + a_-),\\ S_2^- &= -S_2^+ + \sqrt{\frac{2\gamma}{3}}(a_+e^{i\frac{2\pi}{3}} + a_-e^{-i\frac{2\pi}{3}}),\\ S_3^- &= -S_3^+ + \sqrt{\frac{2\gamma}{3}}(a_+e^{i\frac{4\pi}{3}} + a_-e^{-i\frac{4\pi}{3}}).\end{aligned} \tag{23}$$

Let us assume that the structure is excited by a monochromatic signal at frequency $\omega$, incident only from port 1. By plugging $S_1^+ = e^{-i\omega t}$ and $S_2^+ = S_3^+ = 0$ in Eq. (22), we obtain the differential system

$$\begin{aligned}\frac{d^2}{dt^2}a_+ &= -\Omega_\pm^2 a_+ + \chi e^{i\omega_m t}a_- - 2i\omega_\pm\sqrt{\frac{2\gamma}{3}}e^{-i\omega t},\\ \frac{d^2}{dt^2}a_- &= -\Omega_\pm^2 a_- + \chi e^{-i\omega_m t}a_+ - 2i\omega_\pm\sqrt{\frac{2\gamma}{3}}e^{-i\omega t}.\end{aligned} \tag{24}$$

We see that the incident signal couples directly to both $|+\rangle$ and $|-\rangle$ modes, which will therefore necessarily inherit a frequency component at $\omega$. Inspecting Eq. (24) further, it is evident that the time-dependent coupling term between the mode amplitudes will force the $|+\rangle$ mode to have a frequency component at $\omega - \omega_m$, whereas the $|-\rangle$ mode will have a component at $\omega + \omega_m$. We therefore make the following assumption for the solution:

$$\begin{aligned}a_+ &= \alpha_+^0 e^{-i\omega t} + \alpha_+^- e^{-i(\omega-\omega_m)t},\\ a_- &= \alpha_-^0 e^{-i\omega t} + \alpha_-^+ e^{-i(\omega+\omega_m)t},\end{aligned} \tag{25}$$

where the coefficients $\alpha_i^j$ are assumed to be time independent. After plugging (25) into (24), and some straightforward algebra, we obtain the following linear system for the coefficients $\alpha_i^j$:

$$\begin{pmatrix} \Omega_\pm^2-\omega^2 & 0 & 0 & -\chi \\ 0 & \Omega_\pm^2-\omega^2 & -\chi & 0 \\ 0 & -\chi & \Omega_\pm^2-(\omega-\omega_m)^2 & 0 \\ -\chi & 0 & 0 & \Omega_\pm^2-(\omega+\omega_m)^2 \end{pmatrix}\begin{pmatrix}\alpha_+^0\\ \alpha_-^0\\ \alpha_+^-\\ \alpha_-^+\end{pmatrix} = \begin{pmatrix}\sqrt{2\gamma/3}\\ \sqrt{2\gamma/3}\\ 0\\ 0\end{pmatrix}. \tag{26}$$

From the solution of (26), we obtain the components $\alpha_+^0$ and $\alpha_-^0$ of the $|+\rangle$ and $|-\rangle$ modes at $\omega$:

$$\alpha_+^0 = -2i\omega_\pm\sqrt{\frac{2\gamma}{3}}\frac{\Omega_\pm^2-(\omega+\omega_m)^2}{(\omega^2-\Omega_\pm^2)[(\omega+\omega_m)^2-\Omega_\pm^2]-\chi^2}, \tag{27}$$

$$\alpha_-^0 = -2i\omega_\pm\sqrt{\frac{2\gamma}{3}}\frac{\Omega_\pm^2-(\omega-\omega_m)^2}{(\omega^2-\Omega_\pm^2)[(\omega-\omega_m)^2-\Omega_\pm^2]-\chi^2}. \tag{28}$$

We also get the components $\alpha_+^-$ and $\alpha_-^+$, of the $|+\rangle$ and $|-\rangle$ modes, respectively at $\omega - \omega_m$ and $\omega + \omega_m$:

$$\alpha_+^- = -2i\omega_\pm\sqrt{\frac{2\gamma}{3}}\frac{\chi}{(\omega^2-\Omega_\pm^2)[(\omega-\omega_m)^2-\Omega_\pm^2]-\chi^2}, \tag{29}$$

$$\alpha_-^+ = -2i\omega_\pm\sqrt{\frac{2\gamma}{3}}\frac{\chi}{(\omega^2-\Omega_\pm^2)[(\omega+\omega_m)^2-\Omega_\pm^2]-\chi^2}. \tag{30}$$

From the mode amplitudes, we can evaluate the outgoing signals $S_i^-$ using (23). Because they are expressed as linear combinations of the mode amplitudes, these signals contain the excitation frequency $\omega$, as well as its two intermodulation products $\omega \pm \omega_m$. Therefore, after dividing $S_i^-$ by the incident signal $S_1^+ = e^{-i\omega t}$, we extract three different sets of scattering parameters: the set of $S_{ij}^{\omega}$ describing scattering of an incident wave at $\omega$ into outgoing waves at the same frequency $\omega$,

$$\begin{aligned} S_{11}^{\omega} &= -1 + \sqrt{\frac{2\gamma}{3}}(\alpha_+^0 + \alpha_-^0), \\ S_{21}^{\omega} &= \sqrt{\frac{2\gamma}{3}}(\alpha_+^0 e^{i\frac{2\pi}{3}} + \alpha_-^0 e^{-i\frac{2\pi}{3}}), \\ S_{31}^{\omega} &= \sqrt{\frac{2\gamma}{3}}(\alpha_+^0 e^{i\frac{4\pi}{3}} + \alpha_-^0 e^{-i\frac{4\pi}{3}}), \end{aligned} \tag{31}$$

and the sets $S_{ij}^{\omega\pm\omega_m}$, which describe the scattering of a wave at $\omega$ into outgoing waves at frequencies $\omega \pm \omega_m$,

$$\begin{aligned} S_{11}^{\omega+\omega_m} &= \sqrt{\frac{2\gamma}{3}}\alpha_-^+, \\ S_{21}^{\omega+\omega_m} &= \sqrt{\frac{2\gamma}{3}}\alpha_-^+ e^{-i\frac{2\pi}{3}}, \\ S_{31}^{\omega+\omega_m} &= \sqrt{\frac{2\gamma}{3}}\alpha_-^+ e^{-i\frac{4\pi}{3}}, \end{aligned} \tag{32}$$

$$\begin{aligned} S_{11}^{\omega-\omega_m} &= \sqrt{\frac{2\gamma}{3}}\alpha_+^-, \\ S_{21}^{\omega-\omega_m} &= \sqrt{\frac{2\gamma}{3}}\alpha_+^- e^{i\frac{2\pi}{3}}, \\ S_{31}^{\omega-\omega_m} &= \sqrt{\frac{2\gamma}{3}}\alpha_+^- e^{i\frac{4\pi}{3}}. \end{aligned} \tag{33}$$

Equations (31)–(33), together with Eqs. (27)–(30), describe fully the frequency and modulation dependency of the scattering of the system. $S^{\omega}$ describes the scattering of input signals at $\omega$ into output signals at $\omega$, and it is the quantity of interest to predict the isolation performance. The other two matrices $S^{\omega\pm\omega_m}$ describe the conversion of a portion of the input energy at $\omega$ into undesired parasitic output signals at $\omega \pm \omega_m$, which we ideally want to keep at very low levels.

## III. RESULTS

### A. Key performance metrics

The performance of the device can be evaluated using four relevant metrics: (i) the isolation $IS = 20\log|S_{31}^{\omega}/S_{13}^{\omega}|$ of the device, which describes its ability to let an acoustic signal flow from port 1 to 3, but not vice versa. A larger isolation requires a stronger nonreciprocal response; (ii) the forward insertion loss $IL = -20\log|S_{31}^{\omega}|$, which quantifies the signal loss introduced by the device in transmission; (iii) the reflection coefficient $R = 20\log|S_{11}^{\omega}|$; and (iv) the intermodulation strength of the parasitic signals at $\omega \pm \omega_m$, $P = 20\log|S_{31}^{\omega-\omega_m}|$. Ideally, the proposed device should provide large isolation, low insertion loss, low reflection, and low parasitic signals.

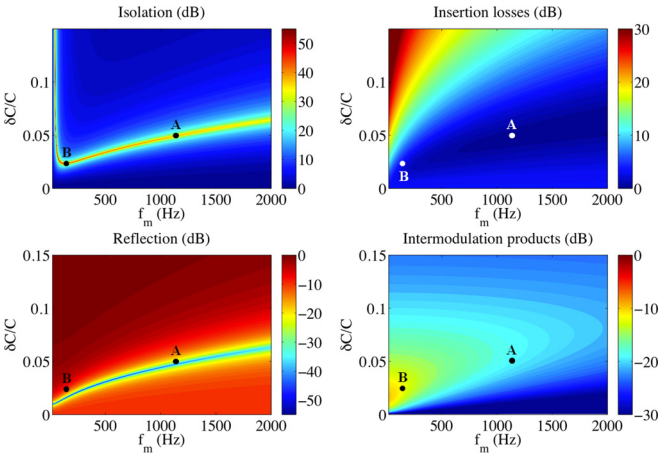


FIG. 3. (Color online) Effect of the modulation depth $\delta C/C$ and modulation frequency $f_m$ on the metrics of the circulator at its resonance frequency $\omega_r$. Top left panel: Isolation. Top right panel: Insertion loss. Bottom left panel: Reflection coefficient. Bottom right panel: Strength of the intermodulation products. Points A and B are two design points considered in the text.

Figure 3 shows contour plots for these quantities, calculated at the resonance frequency $\omega_{\pm}$ of the unbiased resonator, for a range of reasonable values for $f_m \in [0,1500]$ Hz and $\delta C/C_0 \in [0,0.15]$. We assumed cavities 3 mm thick with a diameter of 1 cm, cylindrical internal coupling channels with diameter of 2 mm and 1 mm length, and cylindrical external coupling channels with diameter of 0.5 mm and 1 mm length. The external square waveguides are 3 mm by 3 mm. According to full-wave eigenfrequency simulations, this resonator is characterized by $f_{\pm} = 18628$ Hz and $\gamma = 2\pi\, 76.75\,\mathrm{s}^{-1}$. The top left panel shows the value of $IS$, showing that there is a specific balance between the choice of modulation frequency $f_m$ and depth $\delta C/C_0$ to achieve isolation up to 50 dB. Too slow modulation, with frequencies below 50 Hz, yields high isolation only for unrealistically large values of $\delta C/C_0$, for which our perturbation theory may not even properly hold. By increasing $f_m$ to around 100 Hz, however, it is possible to reach point B in the figure, for which $\delta C/C_0$ has its minimum value $\delta C/C_0 = 2.5\%$, while $IS = 50$ dB is still maximal. By further increasing $f_m$, the required modulation depth slightly increases, and we reach point A in the plot ($\delta C/C_0 = 5\%$, $f_m = 1200$ Hz), for which the value of $IS$ has decreased a bit, down to 40 dB. These two points are of interest for isolation purposes and, to determine the best design, we need to look at the other metrics under the same conditions. For this purpose, we look next at the reflection, shown in the bottom left panel. In order to get low reflections from the device, one needs to operate in the blue region. Interestingly, this blue region and the red region of high $IS$ of the top left panel seem to get closer and closer as $f_m$ increases, which indicates that point A is a better choice in terms of impedance matching, with $R = -40$ dB, as opposed to $R = -10$ dB for point B. A look to the insertion loss and parasitic signals contour plots, respectively, the top right and bottom right panels, confirms the overall ideal operation at point A, for which $IL = 0.3$ dB and $P = -20$ dB, to be compared with $IL = 3$ dB and $P = -12$ dB for point B. This study highlights the importance of tailoring

both modulation depth and frequency, and the tendency of faster modulations to lead to better matching, lower insertion loss, and parasitic signals. Note that the considered values for the modulation frequency are more than an order of magnitude below the working frequency, which makes this design very attractive since many actuating solutions are available at such low frequencies, as we will further discuss in Sec. IV.

### B. A numerical experiment

To confirm the predictions of our analytical model, we performed full-wave simulations of the optimal device using a finite element method and a custom-made frequency domain solver. To model the structure in a full-wave fashion, we need to implement numerically the modulation $\delta C/C_0$ of the cavity capacitance

$$C_0 = V_0\beta_0, \tag{34}$$

where $V_0$ is the volume of any cavity and $\beta_0$ is the compressibility of the acoustic medium that is filling it (here silicon rubber). From Eq. (34) we see that in order to realize the capacitance modulation, we can keep the bulk modulus constant and change the cavity volume. This is the most convenient way to obtain modulation in practice, and it is what we propose here as an experimental solution. By physically compressing the cavity, we would change its volume, but not the bulk modulus (as long as linearity holds, i.e., for small displacements for which Hook's law remains valid), and the change in density would not affect the capacitance, which obviously does not depend on such an inertial quantity. However, this practical way of modulating the capacitance is not the easiest implementation in finite-element simulations, as it involves a dynamically changing geometry and a moving mesh. Instead, we see that we can induce exactly the same effect on the capacitance by keeping the volume constant but modulating the compressibility according to

$$\frac{\delta C}{C_0} = \frac{\delta\beta}{\beta_0}. \tag{35}$$

This is what is implemented in our custom-made finite element solver, and it is strictly equivalent to the practical case of a volume variation with $\beta_0$ constant. To implement our code, we start from the general acoustic equations

$$\begin{aligned} \nabla p(\mathbf{r},t) &= -\frac{d}{dt}[\rho_0\mathbf{u}(\mathbf{r},t)], \\ \nabla\cdot\mathbf{u}(\mathbf{r},t) &= -\frac{d}{dt}[\beta(\mathbf{r},t)p(\mathbf{r},t)], \end{aligned} \tag{36}$$

where $p(\mathbf{r},t)$ is the acoustic pressure, $\mathbf{u}(\mathbf{r},t)$ is the particle velocity, $\rho_0$ is the time independent density of the medium, and

$$\beta(\mathbf{r},t) = \beta_0(\mathbf{r}) + \delta\beta(\mathbf{r})\cos[\omega_m t - \varphi(\mathbf{r})] \tag{37}$$

is the dynamically modulated compressibility of the structure. By taking the divergence of the top equation in (36), and using the bottom equation, we get the wave equation

$$\Delta p(\mathbf{r},t) = \rho_0\frac{d^2}{dt^2}[\beta(\mathbf{r},t)p(\mathbf{r},t)], \tag{38}$$

which is the starting point of our numerical model. Next, since the modulation is periodic in time, we can use Floquet-Bloch theorem and write

$$p(\mathbf{r},t) = f(\mathbf{r},t)e^{i\omega t}, \tag{39}$$

where the function $f$ is periodic in time with period equal to the modulation period,

$$f\left(\mathbf{r},t+\frac{2\pi}{\omega_m}\right) = f(\mathbf{r},t). \tag{40}$$

After a Fourier transform, we have the following expansion for the acoustic pressure:

$$p(\mathbf{r},t) = \sum_n f_n(\mathbf{r})e^{i(\omega+n\omega_m)t}, \tag{41}$$

i.e., the solution of (38) is in general a superposition of a field at $\omega$ and an infinite number of harmonics at $\omega\pm n\omega_m$. By plugging (41) into (38) we transform the initial differential equation with time-dependent coefficient (38) into an infinite linear set of coupled time-independent differential equations, one for each harmonic. We obtain, after some algebra, for an arbitrary harmonic of order $n$,

$$\begin{aligned} &\Delta f_n(\mathbf{r}) + \rho_0\beta(\mathbf{r})(\omega+n\omega_m)^2 f_n(\mathbf{r}) \\ &\quad = -\tfrac{1}{2}\rho_0\delta\beta_0(\mathbf{r})(\omega+n\omega_m)^2[f_{n-1}(\mathbf{r})e^{-i\varphi(\mathbf{r})} + f_{n+1}(\mathbf{r})e^{i\varphi(\mathbf{r})}]. \end{aligned} \tag{42}$$

If the modulation frequency is small, it is reasonable to truncate this infinite system to $n=\{-1,0,1\}$. Then we obtain three coupled differential equations:

$$\begin{aligned} &\Delta f_0(\mathbf{r}) + \rho_0\beta(\mathbf{r})\omega^2 f_0(\mathbf{r}) \\ &\quad = -\tfrac{1}{2}\rho_0\delta\beta_0(\mathbf{r})\omega^2[f_1(\mathbf{r})e^{-i\varphi(\mathbf{r})} + f_1(\mathbf{r})e^{i\varphi(\mathbf{r})}], \\ &\Delta f_{-1}(\mathbf{r}) + \rho_0\beta(\mathbf{r})(\omega-\omega_m)^2 f_{-1}(\mathbf{r}) \\ &\quad = -\tfrac{1}{2}\rho_0\delta\beta_0(\mathbf{r})(\omega-\omega_m)^2 f_0(\mathbf{r})e^{i\varphi(\mathbf{r})}, \\ &\Delta f_1(\mathbf{r}) + \rho_0\beta(\mathbf{r})(\omega+\omega_m)^2 f_1(\mathbf{r}) \\ &\quad = -\tfrac{1}{2}\rho_0\delta\beta_0(\mathbf{r})(\omega+\omega_m)^2 f_0(\mathbf{r})e^{-i\varphi(\mathbf{r})}. \end{aligned} \tag{43}$$

Equations (43) are put in weak form and solved simultaneously in our frequency domain solver. We use scattering boundary conditions at the ports that also include the incident field. The result of our simulation is the field profiles at $\omega$ and $\omega\pm\omega_m$ at any excitation frequency $\omega$, from which we can determine all the scattering parameters and compare the results to the ones of the couple-mode theory analysis [Eqs. (31)–(33)].

Figure 4 shows a comparison between the scattering parameters $S^\omega$ obtained using our coupled mode analytical model and the ones obtained directly from our numerical solver. The agreement between the two methods is excellent. At the resonance frequency $f_\pm = 18\,628$ Hz, both methods predict an isolation $IS = 40$ dB, excellent matching ($R = -40$ dB), small intermodulation products ($P = -20$ dB), and low insertion loss, comparable to the best commercially available radio-frequency circulators ($IL = 0.3$ dB). We stress that this is obtained for acoustic waves, without requiring any magnetic bias, and in a fully linear, parametric (noise-free) device. The only difference between the curves in the figure

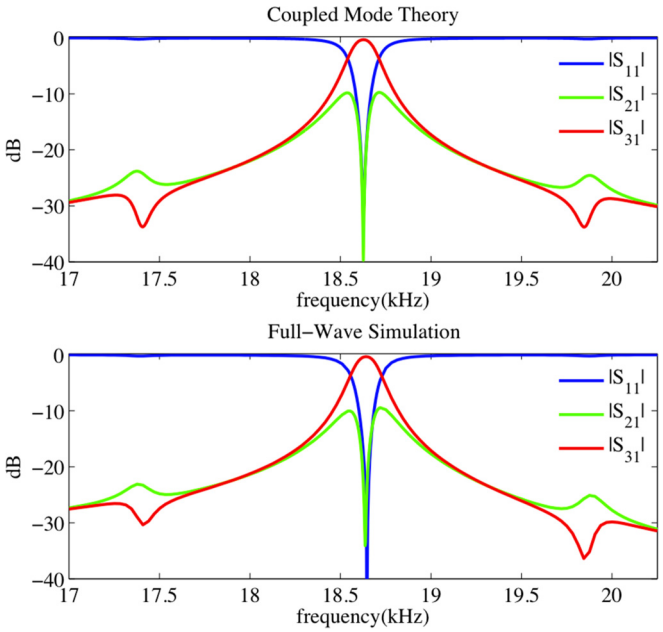


FIG. 4. (Color online) Scattering parameters of the device, for modulation at point A in Fig. 2, versus signal frequency. The analytical results obtained from coupled-mode theory (top) are in excellent agreement with full-wave simulations based on the finite element method (bottom).

is the small asymmetry of the full-wave curves around the design frequency, with slightly higher transmission values at low frequencies, an effect attributed to the presence of the common mode of the resonator at zero frequency, which we have neglected in our analytical calculations.

Figure 5 shows the acoustic pressure field at the resonance frequency, obtained from our numerical simulations, comparing the nonmodulated case [Fig. 5(a)] with the modulated one [Fig. 5(b)], again assuming operation at point A in Fig. 3(a). We assume an ultrasound signal to be incident from port 1: In the

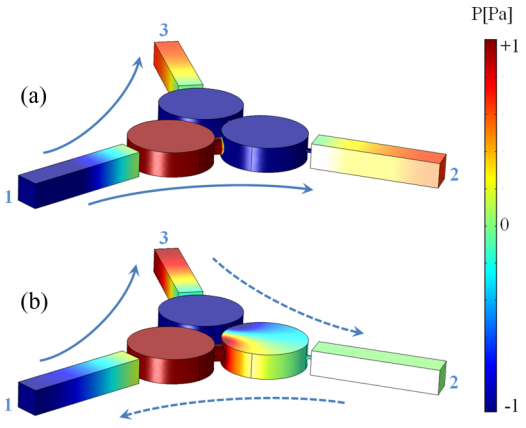


FIG. 5. (Color online) Acoustic pressure field for excitation from port 1. When the modulation is turned off (a), the acoustic signal is evenly split between the output ports 2 and 3. When the spatiotemporal modulation with tailored strength and frequency is turned on (b), it induces strong nonreciprocity by completely routing the acoustic signal to port 3, enabling ultrasonic circulation.

case of the unbiased resonator, the wave splits evenly between the two output ports, with 4/9 of the power transmitted to waveguide 2, 4/9 to waveguide 3, and 1/9 reflected back, due to the 120° rotation symmetry. Due to the reciprocal nature of the unbiased resonator, such a splitting also occurs when the device is excited from port 2 or 3, yielding a symmetric scattering matrix. When the modulation is switched on with the right frequency and depth, the device routes essentially all the impinging power to the port at the left of the input, inducing clockwise nonreciprocal circulation of ultrasound signals, with very small reflection and insertion loss. From port 1, the power goes exclusively to port 3, from port 3 it goes to port 2, and from 2 to port 1, with a handedness that is opposite to the one of the modulation. The coupling between substates $|+\rangle$ and $|-\rangle$, induced by the modulation, generates an intracavity acoustic state that possesses a null of acoustic pressure in cavity 2, preventing any leakage of acoustic energy into the corresponding port. By loading one of the ports with a matched load, it is also possible to turn the circulator into a unique two-port ultrasound isolator.

## IV. DISCUSSION

An important feature of our device is that high levels of isolation are obtained for a signal at 18.5 kHz employing a modulation at a much lower frequency, i.e., 1.2 kHz. According to Fig. 2, even lower modulation frequencies are possible, trading off a bit of insertion loss. For the geometry discussed here, a total displacement of 150 $\mu$m is required to obtain the targeted volume variation of 5%, which is easily achievable at 1200 Hz using conventional actuators. In this frequency range, for instance, piezoelectric ceramics can provide the necessary compression. Considering that the acoustic properties of materials can be modulated much more effectively than the electromagnetic ones (the acoustic index modulation can reach tens of percents in magnetoacoustic crystals [16]), the proposed approach to acoustic nonreciprocity appears particularly attractive for sound and ultrasound applications. In addition, this solution opens exciting opportunities for high-power applications when translated back to the electromagnetic domain, for which conventional magnetic-based circulators cannot be applied, and the electronic modulation considered in recent papers [13,17] would fail.

Our design enables compact and large nonreciprocity with low modulation frequencies and depth, by using a resonant system to boost the interaction between the external acoustic wave and the modulated medium. Therefore, as shown by our coupled-mode theory analysis, the higher the quality factor $Q$, the lower the required modulation depth and frequency for a given performance. In the presence of absorption losses, the $Q$ factor is decreased with respect to the ideal case considered here: on top of radiation losses, we now also have dissipation losses. However, the isolation level of the device can be maintained either by increasing the modulation depth and frequency, or by decreasing the radiation losses by engineering the coupling to the outside waveguides. The level of isolation, which is due to the presence of a destructive interference in front of the output port, does not depend on the presence of losses; however, the modulation requirements to obtain this destructive interference do depend on it.

Nevertheless, we would like to underline that the RTV-602 silicon rubber material assumed here is almost lossless from dc to 1 MHz [15], and we have checked that the results of the full-wave simulations are unaffected by the presence of the small imaginary part in the acoustic index of the medium.

We would like to highlight important differences between this work and Ref. [13], in which a radio-frequency electromagnetic circulator based on a parametrically modulated resonant cavity is reported. In particular, the resonant properties of the acoustic structure considered here are rather different, due to the difference in wave-matter interactions in acoustic resonators. The electromagnetic resonator presented in [13] is obtained by coupling three resonators together, obtaining three different modes by hybridization. Two of them are degenerate and counterpropagating, and are used to create the nonreciprocal effect, while the other one is a pulsing common mode, which can be suppressed by increasing the coupling between the resonant circuits to a very large value (the resonators are indeed connected with short circuits). We then operate near the resonance frequency of the three resonators. In acoustics, it is not possible to create short circuits without affecting irreparably the resonators themselves, and therefore the resonating structure must be completely different. In fact, here the device is operated well below the resonance frequency of the three cavities, which are coupled to each other only weakly. We are working with a lumped resonance mode of the entire loop, and the pulsing mode is forced by nature to resonate at 0 Hz. We use this to our advantage by setting the lumped resonance frequency of the cavity to be far from dc and minimize the effect of the dc mode. In both the electromagnetic and acoustic cases, the design constraints and the associated solutions are directly dictated by the physical nature of the system, which is evidently very different. Therefore, the analytical and numerical modeling of the device are in turn different, as evident by comparing the coupled-mode equations used here with the ones in [13].

While the proposed device does require an external bias, we stress that, from the acoustical standpoint, its functionality is totally passive and the incident acoustic energy is conserved through scattering, i.e., no power is extracted from or absorbed by the modulation. This implies that no energy needs to be provided to the modulation network for the effect to arise, other than the parasitic energy dissipated in the practical implementation of the modulation. In addition, although it supports frequency generation due to time dependency, our system is fully linear and does not violate the superposition principle, as a nonlinear device would, which is largely interesting to avoid signal distortions. With a size below 2.5 cm, our device is as small as $\lambda/6$, which makes it a compact and integrable, noise-free solution for ultrasonic circulation and isolation. It can be tuned in real time to modify the value of isolation, insertion loss, reflection, and even handedness, by simply modifying the modulation depth, frequency, or phase of the modulation signals. Finally, we stress that the proposed concept is very general, and it may be implemented for other types of mechanical waves and in many frequency ranges, from audible sound to thermal phonon frequencies. A broad range of applications can benefit from the concept, spanning acoustic imaging and sonar systems, underwater acoustic communications, vibrational energy concentration and harvesting, signal processing, noise control, heat management via thermal phonon engineering, or telecommunications where our strategy may be used to build isolated delay lines based on surface acoustic waves (SAW) or other types of nonreciprocal SAW devices.

## V. CONCLUSIONS

We have put forward a general concept to achieve isolation and circulation of acoustic signals, relying on rotation imparted by spatiotemporal modulation of the acoustical properties of a composite lumped resonator. We have shown that isolation levels as high as 40 dB can be obtained with an insertion loss as low as 0.3 dB, in a matched ultrasonic device operating at 18.5 kHz, and modulated only by a 5% amplitude at the frequency of 1200 Hz. This work may enable the realization of efficient acoustic or mechanical circulators with industrial applications in transducer technology, acoustic imaging, energy concentration, thermal management, acoustic communication systems, and noise control.

## ACKNOWLEDGMENTS

This work has been supported by the AFOSR Grant No. FA9550-13-1-0204, AFOSR Grant No. FA9550-14-1-0105, and the DTRA Grant No. HDTRA1-12-1-0022. The authors would like to acknowledge Professor A. B. Khanikaev for useful discussions regarding the numerical methods used in this work.

[1] H. Von Helmholtz, *Handbuch der Physiologischen Optik*, 1st ed. (Leopold Voss, Leipzig, 1856), Vol. 1, p. 169.

[2] Lord Rayleigh, Proc. R. Soc. London **4**, 357 (1873).

[3] M. Faraday, *Faraday's Diary*, edited by T. Martin (George Bell and Sons, London, 1933), Vol. IV, Nov. 12, 1839 to June 26, 1847.

[4] B. Lüthi, *Physical Acoustics in the Solid State* (Springer, Berlin, 2007).

[5] J. Heil, B. Lüthi, and P. Thalmeier, Phys. Rev. B **25**, 6515 (1982).

[6] D. Jalas, A. Petrov, M. Eich, W. Freude, S. Fan, Z. Yu, R. Baets, M. Popović, A. Melloni, J. D. Joannopoulos, M. Vanwolleghem, C. R. Doerr, and H. Renner, Nat. Photon. **7**, 579 (2013).

[7] A. A. Maznev, A. G. Every, and O. B. Wright, Wave Motion **50**, 776 (2013).

[8] B. Liang, B. Yuan, and J. Cheng, Phys. Rev. Lett. **103**, 104301 (2009).

[9] N. Boechler, G. Theocharis, and C. Daraio, Nat. Mater. **10**, 665 (2011).

[10] B.-I. Popa and S. A. Cummer, Nat. Commun. **5**, 3398 (2014).
[11] H. B. G. Casimir, Rev. Mod. Phys. **17**, 343 (1945).
[12] R. Fleury, D. L. Sounas, C. F. Sieck, M. R. Haberman, and A. Alù, Science **343**, 516 (2014).
[13] N. A. Estep, D. L. Sounas, J. Soric, and A. Alù, Nat. Phys. **10**, 923 (2014).
[14] D. T. Blackstock, *Fundamentals of Physical Acoustics* (Wiley, New York, 2000).
[15] D. L. Folds, J. Acoust. Soc. Am. **56**, 1295 (1974).
[16] A. P. Brysev, L. M. Krutyanskii, and V. L. Preobrazhenskii, Phys. Usp. **41**, 793 (1998).
[17] D.L. Sounas, C. Caloz, and A. Alù, Nat. Commun. **4**, 2407 (2013).